Longitudinal profiling of B cells primed by mRNA vaccine and recalled by Omicron variants uncovers antibodies broadly neutralizing sarbecoviruses

Xixian Chen[1,2,#], Ling Li[1,#], Ruiping Du[1,2,#], Zuowei Wang[1,#], Yunjian Li[1,2], Yi Sun[1,2], Rongrong Qin[1,2], Hualong Feng[1], Lin Hu[1], Xuanyi Chen[1], Maosheng Lu[1], Xueyan Huang[1], Liwei Jiang[1,*], Teng Zuo[1,*]

[1]Laboratory of Immunoengineering, Institute of Health and Medical Technology, Hefei Institutes of Physical Science, Chinese Academy of Sciences, Hefei 230031, China

[2]University of Science and Technology of China, Hefei 230026, China

[#]These authors contributed equally to this work

*Correspondence: jlw0531@cmpt.ac.cn (L.J.); zuot@cmpt.ac.cn (T.Z.)

Abstract

Regarding to the impact of ancestral SARS-CoV-2 immune imprinting on antibody responses to emerging variants, to what extent memory B cells elicited by wild-type (WT) spike can develop neutralizing breadth and potency in immune recalls is a key question. Here, we longitudinally tracked B cells recognizing WT spike in two individuals of mRNA vaccine, from convalescence of breakthrough infection to acute phase of reinfection. Comprehensive characterization of 632 monoclonal antibodies (mAbs) from those B cells reveals that mAbs cloned after reinfection have dramatically enhanced neutralizing breadth and potency, including 11 mAbs that potently neutralize all tested SARS-CoV-2 variants from WT to KP.3. Among the 11 mAbs, 5 mAbs are classified into public clonotypes encoded by IGHV3-53 or IGHV3-66, whereas the rest belong to a rare clonotype encoded by IGHV3-74. Notably, IGHV3-74 mAbs can even neutralize SARS-CoV-1 with a minimum IC50 of 0.055 μg/ml. Structural and functional analysis further suggests that IGHV3-74 mAbs target a novel epitope on receptor-binding domain, and the best mAb, termed KXD352, is highly resilient to variations on this epitope. Overall, this study demonstrates that both public and rare antibody clonotypes primed by prototype mRNA vaccine can achieve extraordinary neutralizing breadth and potency in repeated Omicron infections.

Introduction

Adaptive immune system adopts multiple mechanisms to ensure specific and diverse antibody responses against various pathogens. During B cell development, V(D)J recombination generates a vast diversity of B cell antigen receptors (BCRs) for naïve B cells (*1*). When infection or vaccination occurs, a small portion of naïve B cell repertoire get activated as their BCRs recognize corresponding antigens by chance (*2*). Activated B cells either differentiate into short-lived plasmablasts (PBs) to produce the initial wave of antibodies, or enter germinal centers (GCs) to undergo repeated rounds of somatic hypermutation and affinity-dependent selection, a process known as antibody affinity maturation (*3*). The evolved GC B cells eventually differentiate into long-lived plasma cells (PCs) to constantly secrete antibodies for months to years, or memory B cells to wait for future encounter with the same or similar antigens (*3*). Compared with primary antigen exposure, secondary antigen exposure typically leads to much faster and stronger antibody responses as recalled memory B cells rapidly differentiate into PB/PCs to secrete high-affinity antibodies (*4*). In addition, memory B cells can be recruited into newly formed GCs to further mature upon secondary antigen exposure (*4*). Overall, these mechanisms work in concert to establish antibody-mediated immune protection against infections.

Since the outbreak of SARS-CoV-2, numerous studies on human antibody responses against spike protein of this emerging virus have been conducted to inform the development of vaccines and antibody therapeutics (*5-7*). Early in the pandemic, extensive isolation and characterization of monoclonal antibodies (mAbs) from convalescents reveals that neutralizing antibodies primarily target epitopes on receptor-binding domain (RBD) and to a lesser extent on N-terminal domain (NTD) of spike (*8, 9*). Furthermore, RBD-specific neutralizing antibodies are categorized into seven major

52 groups according to their binding modes and fine epitopes (*10*), whereas NTD-specific neutralizing
53 antibodies largely target a single supersite (*11, 12*). Although spike-specific antibodies from different
54 convalescents are highly diverse, a series of public antibodies (i.e. antibodies generated by different
55 individuals while sharing common genes and antigen recognition modes) have been widely reported,
56 including antibodies encoded by IGHV3-53, IGHV3-66, IGHV1-58 and IGHV1-69 (*13-16*). In addition,
57 longitudinal profiling of memory B cells from peripheral blood of convalescents demonstrates that
58 spike- or RBD-specific memory B cells display increased somatic hypermutation, binding affinity and
59 neutralizing potency over time, reflecting long-lasting GC responses elicited by primary SARS-CoV-2
60 infection (*17-19*). Compared with SARS-CoV-2 infection, two doses of SARS-CoV-2 mRNA vaccines
61 lead to equivalent plasma neutralizing activity and similar amount of RBD-specific memory B cells
62 (*20*). Spike- or RBD-specific mAbs cloned from vaccinees and convalescents recognize common
63 epitopes and share frequently-used antibody genes (*20*). Moreover, analysis of draining lymph node
64 samples from vaccinees indicates that mRNA vaccines provoke persistent GCs, which last for at least
65 six months and enable the maturation of spike-specific B cells (*21, 22*).
66 Under the immune pressure established by infection and vaccination, SARS-CoV-2 variants,
67 represented by Alpha (B.1.1.7), Beta (B.1.351), Gamma (P.1), Delta (B.1.617.2) and Omicron
68 (B.1.1.529), emerged successively in the first two years of the pandemic. Among them, Omicron
69 exhibited most striking evasion to neutralizing antibodies induced by ancestral SARS-CoV-2 spike
70 and therefore caused a new wave of infections worldwide (*23*). Omicron infection in individuals
71 administrated with mRNA vaccines predominantly recalls cross-reactive memory B cells elicited by
72 vaccination whereas rarely induces *de novo* Omicron-specific B cells responses, highlighting that
73 ancestral SARS-CoV-2 imprints B cell responses to Omicron (*24-27*). Consequently, plasma

74 neutralizing activity against ancestral SARS-CoV-2 and Omicron are enhanced synchronously (*24-*
75 *27*). Moreover, B cell clones with more mutations and higher affinities towards Omicron progressively
76 remodel spike-specific memory B cell repertoire, suggesting that cross-reactive memory B cells can
77 undergo further affinity maturation in new GCs induced by Omicron breakthrough infection (*28, 29*).
78 With the rapid emergence of Omicron-derived variants, such as BA.2.75, BA.5, BF.7, BQ.1, XBB.1.5,
79 XBB.1.16, EG.5.1, BA.2.86 and JN.1, repeated infections with these variants have become common
80 and updated vaccines have been applied accordingly in some countries (*30*). In individuals with prior
81 exposures to wild-type (WT) spike, antibody responses boosted by subsequent exposures to
82 emerging Omicron variants, either through infection or vaccination, display biased neutralizing
83 activities to ancestral SARS-CoV-2 and earlier Omicron variants, suggesting that immune imprinting
84 may impede the elicitation of neutralizing antibodies against more recent and future variants (*31-35*).
85 Nonetheless, mAbs from those individuals dramatically surpass mAbs elicited by WT spike in
86 neutralizing breadth and potency, indicating that immune imprinting is potentially beneficial for the
87 development of broadly neutralizing antibodies (bnAbs) (*28, 36*).
88 As the evolution of SARS-CoV-2 shows no signs of stop, repeated exposures to emerging SARS-
89 CoV-2 variants will constantly happen in the future. Regarding to the impact of ancestral SARS-CoV-
90 2 immune imprinting on antibody responses to emerging variants, to what extent memory B cells
91 elicited by WT spike can develop neutralizing breadth and potency in immune recalls is a key question.
92 To address this question, we performed a 7-month longitudinal study of B cells recognizing WT spike
93 in two individuals of mRNA vaccine, from convalescence of breakthrough infection to acute phase of
94 reinfection. Functional and genetic analysis of 632 mAbs from those B cells reveals that mAbs cloned
95 after reinfection have dramatically enhanced neutralizing breadth and potency, which is likely due to

96 recall of pre-existing memory B cells and maturation of those cells either before or after reinfection.
97 Among the 11 mAbs that potently neutralize all tested SARS-CoV-2 variants from WT to KP.3, 5 mAbs
98 are classified into public clonotypes encoded by IGHV3-53 or IGHV3-66, whereas the rest belong to
99 a rarely reported clonotype encoded by IGHV3-74. Notably, IGHV3-74 mAbs can even neutralize
100 SARS-CoV-1 with a minimum IC50 of 0.055 μg/ml. Structural and functional analysis shows that
101 IGHV3-74 mAbs can block the binding between RBD and ACE2 by targeting a novel epitope
102 consisting of E340-R346, V367-S375, N436-G446 and Q498-V503. Moreover, the best IGHV3-74
103 mAb, termed KXD352, is highly resilient to variations on this epitope. Overall, this study demonstrates
104 that both public and rare antibody clonotypes primed by ancestral SARS-CoV-2 mRNA vaccine have
105 potential to achieve extraordinary neutralizing breadth and potency in repeated Omicron infections.

106 **Results**

107 **Reinfection enhances plasma neutralizing antibody responses**

108 In our previous study, we recruited a cohort to study antibody responses elicited by breakthrough
109 infection (*37*). Among them, Donor 1 and 2 received two doses of mRNA vaccines in the middle or
110 beginning of 2021 and were infected by BA.5 or BF.7 in the end of 2022 (Figure 1A). With their blood
111 samples collected about two months (T1) after infection, we have identified multiple mAbs with broadly
112 neutralizing capacity (*37*). To longitudinally track B cell responses in these two donors, we also
113 collected blood samples about 3 months (T2) and 6 months (T3) after infection. Donor 1 showed
114 symptoms of infection and was confirmed by SARS-CoV-2 antigen test on August 25 2023, when
115 EG.5.1 caused a new round of infections in China (*38*). Eleven days later (T4), blood was collected
116 again from Donor 1 to study acute phase antibody responses evoked by reinfection. In parallel, we

117 also collected blood from Donor 2 at T4, though Donor 2 reported no symptoms and negative test
118 results during several waves of infections before this time point.

119 We measured neutralizing antibody titers of plasma from four time points against a panel of 18
120 pseudoviruses bearing spikes from ancestral SARS-CoV-2 (WT), Alpha, Beta, Gamma, Delta, BA.1,
121 BA.4/5, BA.2.75, BQ.1, XBB, XBB.1.5, EG.5.1, HK.3, BA.2.86, JN.1, KP.2, KP.3 and SARS-CoV-1
122 (Figure 1B and Figure S1). Overall, the plasma neutralizing titers (NT50s) of both donors gradually
123 decrease from T1 to T3 with a maximum of 10.7 folds. After reinfection, plasma from Donor 1 at T4
124 shows substantially increased neutralizing titers against most strains by a maximum of 20.7 folds
125 compared to T3. The titers of plasma from Donor 2 continuously decline or sustain from T3 to T4 for
126 most strains, whereas increase by 1.9 to 2.7 folds for strains including Gamma, BA.1 and XBB. As
127 latest variants of XBB and BA.2.86 lineages, HK.3 and KP.3 are least sensitive to neutralization,
128 highlighting the continuous neutralization escape (Figure 1C). Nonetheless, plasma at T4 from Donor
129 1 displays relatively stable neutralizing titers across all SARS-CoV-2 variants, indicating that
130 reinfection enhances the breadth of neutralizing antibody response in Donor 1.

131 **Monoclonal antibodies cloned from WT-spike-specific B cells after reinfection exhibit**
132 **improved neutralizing breadth and potency**

133 As memory B cells elicited by ancestral SARS-CoV-2 mRNA vaccine typically maintain their
134 specificities to WT spike in recalled responses (*24-29, 31-35*), we used WT-spike as bait to track
135 memory B cells initially induced by mRNA vaccine in peripheral blood mononuclear cells (PBMCs)
136 from these two donors. Consistent with plasma neutralizing titers, the frequencies of WT-spike-
137 specific B cells in Donor 1 drop sequentially from T1 to T3 and then rise back to initial level (Figure

138 2A). Unexpectedly, Donor 2 displays similar dynamic changes as Donor 1, suggesting that Donor 2
139 may have experienced an asymptomatic infection between T3 and T4.

140 To examine the binding and neutralizing properties of antibodies from those WT-spike-specific B
141 cells, we cloned the variable regions of antibodies from those B cells into expression vectors through
142 single-cell RT-PCR. Then we transfected HEK293T cells with those vectors and harvested
143 supernatant for ELISA and neutralization assay (Figure 2B). In ELISA, the supernatant was tested
144 with RBD, NTD, S1, S2 and spike (S) from WT SARS-CoV-2 and spikes from Omicron variants
145 including BA.4/5, XBB.1.5, EG.5.1 and JN.1. In neutralization assay, the supernatant was tested
146 against WT, BA.4/5, XBB.1.5, EG.5.1 and JN.1 pseudoviruses.

147 With published mAbs at T1 included, we identified 448 and 184 WT-spike-specific mAbs from Donor
148 1 and Donor 2 respectively. The main targets of these mAbs are RBD, NTD and S2, with the
149 proportions of mAbs to each domain slightly varying from T1 to T4 (Figure 2C). Regarding to cross-
150 binding with different spikes, the frequencies of RBD-specific mAbs that bind WT and one Omicron
151 variant, either BA.4/5, XBB.1.5, EG.5.1 or JN.1, decline from T1 to T3 and then ascend (Figure 2D,
152 Figure S2A). However, similar trend is not observed in NTD- and S2-specific mAbs.

153 By defining 70% inhibition as cutoff, we identified 127 mAbs that are able to neutralize WT
154 pseudoviruses (WT-neutralizing mAbs), with 77 from Donor 1 and 50 from Donor 2 (Figure 2E).
155 Among them, only 5 mAbs target NTD while the others exclusively recognize RBD. Regarding to
156 cross-neutralizing activity, around 20-30% of mAbs at T4 are able to neutralize all 5 tested
157 pseudoviruses, whereas only 2 out of 61 mAbs from T1 to T3 have such capacity (Figure 2F).
158 Moreover, the frequencies of mAbs that cross-neutralize WT and one Omicron variant drop from T1
159 to T3 and then jump to highest levels at T4 (Figure 2G, Figure S2B).

160 To further compare the breadth and potency of neutralizing mAbs from different time points, we
161 purified those mAbs and measured their IC50s against 14 representative pseudoviruses including
162 WT, Delta, BA.1, BA.4/5, BA.2.75, BQ.1, XBB.1.5, EG.5.1, HK.3, BA.2.86, JN.1, KP.2, KP.3 and
163 SARS-CoV-1 (Figure 3A). Four neutralizing mAbs screened by supernatant were not included in this
164 analysis because of low yields. Among all tested mAbs, 4 mAbs from Donor 2 are able to neutralize
165 all SARS-CoV-2 variants and SARS-CoV-1. In addition, 2 mAbs from Donor 1 and 5 mAbs from Donor
166 2 can neutralize all SARS-CoV-2 variants from WT to KP.3. Notably, these 11 mAbs are exclusively
167 identified from PBMCs collected at T4. Along with this finding, differences are observed in the overall
168 neutralizing breadth of mAbs at T1 to T4 (Figure 3B, Figure S3A). T1 and T4 have higher frequencies
169 of neutralizing antibody against BA.1, BA.4/5, BA.2.75, BQ.1, XBB.1.5 and BA.2.86 than T2 and T3,
170 which is consistent with neutralization results of supernatant. Moreover, T4 has higher proportions of
171 neutralizing antibody against EG.5.1, HK.3, JN.1, KP.2 and KP.3 than the other time points.
172 Regarding to neutralizing potency, the overall IC50s of mAbs at T4 are lower than that of mAbs at
173 T2 and T3 against most strains (Figure 3C, D, Figure S3A). In addition, mAbs at T4 also display
174 superior neutralizing potency than mAbs at T1 against Delta, EG.5.1, HK.3, JN.1 and KP.2. In contrast,
175 significant differences in IC50s are generally not observed among mAbs at T1 to T3 by statistical
176 analysis. We also combined mAbs at T1 to T3 together and compared them with mAbs at T4, which
177 further confirms that mAbs isolated after reinfection have superior neutralizing breadth and potency
178 than mAbs before reinfection (Figure S3B-D). Taken together, these data suggest that mAbs cloned
179 from WT-spike-specific B cells after reinfection have enhanced neutralizing breadth and potency.
180 **Reinfection recalls pre-existing memory B cells**

181 To explain the enhanced neutralizing breadth and potency of mAbs cloned after reinfection, we moved
182 on to analyze the sequences of mAbs from T1 to T4. Binding mAbs from both donors use a wide
183 range of V genes (Figure 4A, B). The frequencies of each V gene from T1 to T4 are more consistent
184 for mAbs from Donor 1 than those from Donor 2, likely due to fewer mAbs isolated from Donor 2 at
185 T2 and T3. The most frequently-used V genes for heavy chain include IGHV3-30, IGHV3-66, IGHV3-
186 53, IGHV3-33, IGHV1-69 and IGHV1-46. Among them, IGHV3-30 and IGHV3-33 are primarily used
187 by mAbs targeting S2, whereas IGHV3-66, IGHV3-53 and IGHV1-69 are preferentially used by mAbs
188 recognizing RBD (Figure S4A). The most frequently-used V genes for light chain include IGKV1-39,
189 IGKV3-20, IGKV3-15, IGKV3-11, IGKV1-33, IGKV1-5 and IGKV1-9, which are less biased toward
190 mAbs targeting a certain domain than V genes for heavy chain (Figure S4A). In contrast to binding
191 mAbs, neutralizing mAbs are predominantly encoded by IGHV3-66, IGHV3-53 and IGHV1-69 (Figure
192 4A, B). Furthermore, in these neutralizing mAbs, IGHV3-66 and IGHV3-53 typically pair with IGKV1-
193 33, IGKV1-9 and IGKV3-20, whereas IGHV1-69 commonly pair with IGLV1-40 (Figure S4B). It is
194 worth mentioning that the pair of IGHV3-74 and IGKV3-20 is used by 10 out of 50 neutralizing mAbs
195 from Donor 2. Nonetheless, the overall profiles of V gene usage are rather consistent from T1 to T4.
196 According to V and J genes and CDR3 similarity, we defined 401 and 145 unique clonotypes
197 respectively from 448 and 184 mAbs (Figure 4C). The expanded clonotypes are primarily found in
198 mAbs at T4, particular for Donor 2, further indicating that T4 is also in acute phase of reinfection for
199 Donor 2. As an evidence of recall of pre-existing memory B cells, multiple clonotypes found at T1 to
200 T3 are extensively expanded at T4, particular for neutralizing clonotypes such as Clonotype 204 and
201 223 from Donor 1 and Clonotype 88 and 92 from Donor 2 (Figure 4D).

202 On the other hand, mAbs at T4 have more somatic mutations than those from earlier time points,
203 which can be either due to recall of pre-existing memory B cells with more mutations, or due to further
204 maturation of pre-existing memory B cells in new GC reactions (Figure 4E). Taken together, these
205 data suggest that the enhanced neutralizing breadth and potency of mAbs at T4 is attributed to recall
206 of pre-existing memory B cells and maturation of those cells either before or after reinfection.

207 **Both public and rare antibody clonotypes can develop extraordinary neutralizing breadth and**
208 **potency**

209 After longitudinal analysis of overall B cell responses in these two donors, we moved on to
210 characterize the 11 mAbs with extraordinary neutralizing breadth (Figure 3A, Figure 5A). Clonotype
211 analysis reveals that they belong to 5 unique clonotypes including Clonotype 92, 82 and 75 from
212 Donor 2 and Clonotype 240-2 and 212-1 from Donor 1. Clonotype 92 is encoded by IGHV3-74 and
213 IGHV3-20, which is rarely reported in RBD-specific antibodies against SARS-CoV-2 (*16*). This
214 clonotype contains 10 neutralizing mAbs, with 1 from T2 and 9 from T4. Among them, KXD350,
215 KXD352, KXD355 and KXD358 can neutralize all tested viruses while KXD371 and KXD372 can
216 neutralize all SARS-CoV-2 variants. The other 4 mAbs in this clonotype are completely escaped by
217 at least one SARS-CoV-2 variant. With IC50s ranging from 0.002 to 0.008 μg/mL against SARS-CoV-
218 2 variants and IC50 of 0.055 μg/mL against SARS-CoV-1, KXD352 ranks as the best neutralizing
219 mAb in this study. According to the phylogenetic tree, mAbs in this clonotype can be divided into two
220 major clades, suggesting that neutralizing breadth can be developed through diverse evolution
221 pathways.

222 The other four clonotypes belong to previously defined IGHV3-53/3-66 public antibody clonotypes
223 (*16*). Clonotype 82 is encoded by IGVH3-66 and IGKV1-33 and contains 8 neutralizing mAbs from

224 T4. However, only KXD357 is able to neutralize all SARS-CoV-2 variants, with IC50s ranging from
225 0.003 to 0.224 μg/ml. Similar as Clonotype 92, Clonotype 82 also has two major clades. Although
226 mAbs in both clades are extensively mutated, mAbs in Clade-2 exhibit superior neutralizing breadth
227 than mAbs in Clade-1. Encoded by IGHV3-53 and IGKV3-15, Clonotype 75 contains previously
228 published KXD02 from T1 and two addition mAbs from T4. In our previous study, we have shown that
229 KXD02 broadly neutralizes SARS-CoV-2 variants from WT to HK.3 (*37*). However, KXD02 is soon
230 escaped by variants in BA.2.86 lineages including JN.1, KP.2 and KP.3. In contrast, KXD353 and
231 KXD356 from T4 maintain neutralizing activities against all SARS-CoV-2 variants, with IC50s ranging
232 from 0.002 to 0.216 μg/ml. In line with increased neutralizing breadth and potency, KXD353 and
233 KXD356 are also more evolved than KXD02 according to phylogenetic analysis. As singletons from
234 Donor 1, Clonotype 240-2 (KXD470) is encoded by IGHV3-66 and IGKV1-9, whereas Clonotype 212-
235 1 (KXD472) is encoded by IGHV3-53 and IGKV1-5. Although both mAbs are able to neutralize all
236 SARS-CoV-2 variants, they are less potent to KP.2 and KP.3 than bnAbs from Donor 2.

237 As all these clonotypes are identified with WT spike, we assume that they are initially primed by
238 ancestral SARS-CoV-2 mRNA vaccine but not by BA.5 or BF.7 breakthrough infection. To confirm
239 this assumption, we synthesized the putative germline antibodies of each clonotypes and measured
240 their binding avidities to WT and BA.4/5 spikes expressed on HEK293T cells (Figure 5B). BF.7 was
241 not tested since it has only one amino acid different from BA.5 in RBD. All the germlines, except GL-
242 4, show strong to moderate binding to WT spike. In contrast, they all display weak or even
243 undetectable binding to BA.4/5 spike. The biased recognition towards WT spike suggest that these
244 clonotypes are more likely to be activated by mRNA vaccine. Taken together, these data suggest that

245 both public and rare antibody clonotypes primed by ancestral SARS-CoV-2 mRNA vaccine have
246 potential to develop ultra-broad and potent neutralizing activities in repeated Omicron infections.

247 **IGHV3-74-encoded bnAbs target a novel epitope and exhibit dramatic resilience to mutations**
248 **on the epitope**

249 To evaluate the neutralizing potential of these mAbs to future SARS-CoV-2 variants, we moved on to
250 explore the structural basis for their neutralizing breadth. We first performed competition ELISA to
251 roughly map their epitopes with ACE2, CR3022, S309, P2S-2E9, BD55-5483, BD56-1854 and BD55-
252 1205 as references (Figure 6A). As reported, CR3022 binds to a cryptic epitope on the inner face of
253 RBD whereas S309 recognizes N343 proteoglycan epitope on the outer face of RBD (Figure S5A)
254 (*39, 40*). P2S-2E9 and BD55-5483 (analogue of BD55-5514) both target the previously defined "mesa"
255 of RBD, respectively biased to the outer face and inner face (*10, 41, 42*). As representatives of IGHV3-
256 53/3-66 public antibodies, BD56-1854 and BD55-1205 target receptor-binding-motif (RBM) (*43*).

257 We tested four SARS-CoV-1-neutralizing mAbs (KXD350, KXD352, KXD355 and KXD358) from
258 Clonotype 92 (IGHV3-74 mAbs) and five mAbs (KXD353, KXD356, KXD357, KXD470 and KXD472)
259 from other clonotypes (IGHV3-53/3-66 mAbs) (Figure 6A). IGHV3-53/3-66 mAbs compete with BD55-
260 5483, BD56-1854 and BD55-1205 but not with S309 and P2S-2E9. In contrast, IGHV3-74 mAbs
261 compete with S309, P2S-2E9 and BD55-5483 while not with BD56-1854 and BD55-1205. Moreover,
262 no competition is observed between these mAbs and CR3022 except for some minor competition
263 between KXD358 and CR3022. In addition, they all compete with ACE2, suggesting that they
264 neutralize SARS-CoV-2 through receptor blockade.

265 To define the fine epitopes of these mAbs, we performed structure prediction with AlphaFold 3. The
266 predicted structures of IGHV3-53/3-66 mAbs in complex with WT RBD are similar to the structure of

267 BD55-1205 in complex with XBB.1.5 RBD (Figure S5B). According to these structures, we defined
268 the common epitope of IGHV3-53/3-66 mAbs, which largely overlap with the epitope of ACE2 (Figure
269 6B, C).

270 On the other hand, AlphaFold 3 generated various structures for the complexes of IGHV3-74 mAbs
271 and WT RBD. However, only one type of structures is consistent with epitope mapping by competition
272 ELISA. Here, KXD355 is taken as an example to present the results. Binding to the previously defined
273 "escarpment" of RBD (*10*), KXD355 clashes with S309, P2S-2E9 and BD55-5514 (analogue of BD55-
274 5483) but not with BD55-1205 and CR3022 (Figure S5C). As this epitope is exposed on both up and
275 down RBDs, KXD355 can bind RBDs in both conformations (Figure 6D). In details, the long CDRH3
276 of KXD355 extends into a groove formed by three helixes on the "escarpment" of RBD (Figure 6E).
277 Meanwhile, the other CDRs attach to "mesa" of RBD to provide support for CDRH3. Accordingly, the
278 epitope of KXD355 includes 22 residues distributed on E340-R346, V367-S375, W436-G446 and
279 Q498-V503 (Figure 6F).

280 To confirm the predicted epitopes, we constructed a panel of single-mutated KP.3 spikes and
281 measured their escape to those mAbs in binding and neutralization (Figure 6G). Compared to KP.3,
282 most mutants show similar or slightly lower expression levels on HEK293T cells, which is indicated
283 by a NTD-specific mAb. In contrast, nearly half of these mutants display reduced binding to ACE by
284 different extent. Regarding to the binding with mAbs, mutants including K403D, D420N, Y421K,
285 L456V, L456S, K460F, A475V, N487K, Y489A, Y489D, R498A and R498D completely lose binding
286 to at least one IGHV3-53/3-66 mAb. To a lesser extent, mutants like N343A, N343F, K440D, L441S
287 and H445D show decreased binding to IGHV3-74 mAbs. Consistent with reduced binding, the
288 aforementioned mutants also display dramatic escape of neutralization to corresponding mAbs. In

289 addition, mutants such as T345A, T345F, K444A and K444D are also resistant to certain IGHV3-74
290 mAbs, although they only partially lose binding to those mAbs. It is worth mentioning that KXD352 is
291 only completely escaped by L441S, which also impairs ACE2 binding, whereas maintain low IC50s
292 against all the other mutants (Figure S6). In addition, although SARS-CoV-1 has more than 10
293 mutations on the epitope of IGHV3-74 mAbs compared with SARS-CoV-2 variants, KXD352 can
294 neutralize SARS-CoV-1 with a low IC50 of 0.055 μg/ml, highlighting that KXD352 is highly resilient to
295 variations on its epitope (Figure 5A, Figure S7A).

296 To evaluate the likelihood that these mAbs are escaped by future circulating SARS-CoV-2 strains,
297 we collected 25332 spike sequences published between June 1 to October 1 in 2024. With KP.3 as
298 reference, we analyzed the mutations on the epitopes of these bnAbs (Figure 6H, Figure S7B). With
299 extremely low frequency, multiple confirmed escape mutations for IGHV3-53/3-66 mAbs are found in
300 the circulating strains, including D420N (0.0079%), A475V (0.02882%), N487K (0.0079%). In contrast,
301 confirmed escape mutations for IGHV3-74 mAbs are not found in the circulating strains. Overall, these
302 data predict that IGHV3-74 mAbs, particular KXD352, will not be easily escaped by SARS-CoV-2 in
303 near future.

304 **Discussion**

305 The key scientific question of this study is to what extent memory B cells elicited by WT spike can
306 develop neutralizing breadth and potency in immune recalls. Strategically, we used WT spike as bait
307 to track those B cells as they typically maintain specificities to WT spike in immune recalls (24-29, 31-
308 35). A recent study pointed out that pre-existing memory B cells induced by ancestral SARS-CoV-2
309 could redirect their specificities to emerging variants in repeated Omicron exposures (*44*). As our
310 focus was memory B cells broadly recognizing SARS-CoV-2 from WT to emerging variants, we did

311 not take into account those memory B cells with redirected specificities. Regarding to the samples,
312 we collected blood from 2 individuals of mRNA vaccines at four time points, which are 2 months, 3
313 months, 6 months and 9 months after BA.5 or BF.7 breakthrough infection. In addition, Donor 1
314 experienced a symptomatic reinfection at 11 days before the last time point, while Donor 2
315 experienced an asymptomatic reinfection shortly before the last time point, as suggested by our data.
316 Therefore, the timeline of this longitudinal study is ranging from convalescence of breakthrough
317 infection to acute phase of reinfection, which enables us to track the evolution of memory B cells
318 elicited by ancestral SARS-CoV-2 mRNA vaccine in repeated Omicron infections.

319 A major finding of this study is that mAbs cloned after reinfection have superior neutralizing breadth
320 and potency, which is accompanied with expansion of pre-existing clonotypes and increased mutation
321 levels. According to the antigen exposure history of these two donors, this finding can be explained
322 by two possibilities. First, a fraction of pre-existing memory B cells, which have already undergone
323 extensive maturation and developed superior neutralizing breadth and potency, are recalled by
324 reinfection. Second, a fraction of pre-existing memory B cells are recalled by reinfection and then
325 acquire further maturation in new GC responses. Non-mutually exclusive, these two possibilities differ
326 in whether an addition round of maturation occurs after reinfection. Previous studies suggest that
327 BA.1 breakthrough infection or booster vaccination can both lead to affinity maturation of pre-existing
328 memory B cells induced by mRNA vaccines (*28, 29, 45*). Here, we are not able conclude whether
329 memory B cells induced by mRNA vaccines can undergo two rounds of affinity maturation sequentially
330 driven by breakthrough infection and reinfection. We plan to address this issue by long-term tracking
331 of WT-spike-specific B cells after reinfection in these two donors.

332 A highlight of this study is the identification of 4 bnAbs against SARS-CoV-2 and SARS-CoV-1.

333 These bnAbs belong to a clonotype encoded by IGHV3-74, which is rarely used by RBD-specific
334 antibodies (*16*). Structural analysis indicates that these IGHV3-74 bnAbs bind to an epitope consisting
335 of E340-R346, V367-S375, N436-G446 and Q498-V503. In an early study, epitopes on RBD are
336 classified into seven groups, with RBD-1 to RBD-3 on the top face, RBD-4 and RBD-5 on the outer
337 face, RBD-6 and RBD-7 on the inner face (*10*). More recently, a cryptic epitope recognized by human
338 mAb BIOLS56 and IMCAS74 is defined as RBD-8 (*46*). Referred to these epitope categories, the
339 epitope of these IGHV3-74 bnAbs stretches across RBD-3 and RBD-5 and is therefore a novel epitope.
340 Identification of escape mutations demonstrates that KXD352 is highly resilient to variations on this
341 epitope. According to structures predicted by AlphaFold 3, we speculate that this resilience is due to
342 the plasticity of its long CDRH3, which plays a key role in contacting with its epitope.

343 As a byproduct of defining a novel broadly neutralizing epitope on RBD, our study represents an
344 example of epitope mapping with AlphaFold 3. In our practice with AlphaFold 3, it is straightforward
345 to predict the structures of IGHV3-53/3-66 mAbs, probably because the structures of similar
346 antibodies have been reported in a large amount. In contrast, various structures are predicted for
347 IGHV3-74 bnAbs. In this case, traditional epitope mapping with competition ELISA is necessary to
348 pick the best candidates for further confirmation. Overall, our attempt to apply AlphaFold 3 in fine
349 epitope mapping turned out to be successful.

350 Similar to a preprint posted recently (*47*), we identified multiple IGHV3-53/3-66 public antibodies
351 with ultra-broad neutralizing activities against SARS-CoV-2. In addition, we observed the expansion
352 of clonotypes encoded by IGHV3-53/3-66. According to phylogenetic analysis, the improved
353 neutralizing breadth and potency of IGHV3-53/3-66 public antibodies is somehow not always
354 correlated to the extent of somatic hypermutation, supporting the view that bystander mutations

355 generated in a stochastic manner are critical for the development of bnAbs against SARS-CoV-2 (*48,*
356 *49*).

357 Currently, ancestral SARS-CoV-2 immune imprinting has been acknowledged as a great challenge
358 for the update of SARS-CoV-2 vaccines (*32-35*). In one preprint we posted recently, we find that
359 immune imprinting can facilitate the development of bnAbs against SARS-CoV-2 (*50*). Here, we
360 further show that memory B cells elicited by prototype mRNA vaccine have potential to develop
361 exceptional neutralizing breadth and potency. Together, our studies suggest that vaccines based on
362 emerging variants are able to enhance antibody responses against current and future variants in the
363 presence of immune imprinting. From the aspect of antibody therapeutics, KXD352 exhibits broad
364 and potent neutralizing activity against SARS-CoV-2 and SARS-CoV-1. In addition, KXD352 targets
365 a novel epitope and tolerates mutations on this epitope. Therefore, KXD352 is an ideal candidate for
366 antibody therapeutics against future SARS-CoV-2 variants and related sarbecoviruses.

367 **Materials and methods**

368 **Ethics statement**

369 This study was approved by the Ethics Committee of Hefei Institutes of Physical Science, Chinese
370 Academy of Sciences (Approval Number: YXLL-2023-47). All donors provided written informed
371 consent for collection of information, analysis of plasma and PBMCs, and publication of data
372 generated from their samples.

373 **Human samples**

374 Peripheral blood samples were collected from 2 donors. Plasma and PBMCs were isolated from blood
375 through Ficoll density gradient centrifugation.

376 **Protein expression and purification**

377 The extracellular domains of spikes from WT, BA.4/5, XBB.1.5, EG.5.1, JN.1 were constructed with a
378 foldon-trimerization-motif, a His-tag, a tandem Strep-tag II and a FLAG-tag at C-terminal. S1, NTD
379 and RBD of WT spike were constructed with a Strep-tag II at C-terminal. S2 of WT spike was
380 constructed with a His-tag at C-terminal. Human ACE2 (huACE2, 1-740) was constructed with a
381 Strep-tag II at N-terminal. All recombinant proteins were expressed in FreeStyle 293F cells and
382 purified with Streptactin Agarose Resin 4FF (Yeasen, 20495ES60) or Ni-NTA Agarose (Qiagen,
383 30210).

384 **Cloning and expression of mAbs**

385 As previously described (*37*), PBMCs were first incubated with 200nM WT spike. After wash, cells
386 were stained with antibodies targeting CD3, CD19, CD27, CD38, human IgM, human IgD, His-tag
387 and FLAG-tag along with DAPI. WT-spike-specific B cells were gated as $DAPI^{-}CD3^{-}CD19^{+}CD27^{+}IgD^{-}$
388 $His^{+}FLAG^{+}$ and sorted into 96-well PCR plates with one cell per well. After reverse transcription
389 reaction, variable regions of antibody heavy and light chains from single B cells were amplified by
390 nested PCR and cloned into human IgG1 expression vectors. Paired heavy and light chain plasmids
391 were co-transfected into HEK293T cells or FreeStyle 293F cells. Antibodies were purified with Protein
392 A magnetic beads (GenScript, L00273).

393 **ELISA**

394 Indicated antigens were coated onto 96-well ELISA plates (100 ng/well) at 4˚C overnight. After
395 blocking with blocking buffer (PBS with 10% FBS), undiluted HEK293T supernatant was added to the
396 wells and incubated at 37˚C for 1hr. After wash, HRP-conjugated goat anti-human-IgG antibodies
397 (Zen-bio, 550004) were added and incubated at 37˚C for 1hr. After wash, TMB substrate (Sangon
398 Biotech, E661007-0100) was added and incubated at room temperature for 5 minutes. Then the

399 reaction was stopped with stop solution and absorbance at 450 nm (OD450) was measured.

400 **Pseudovirus neutralization assay**

401 To generate pseudoviruses, HEK293T cells were transfected with psPAX2, pLenti-luciferase and
402 spike-encoding plasmids (WT, Alpha, Beta, Gamma, Delta, BA.1, BA.4/5, BA.2.75, BQ.1, XBB,
403 XBB.1.5, EG.5.1, HK.3, BA.2.86, JN.1, KP.2, KP.3, SARS-CoV-1 and KP.3 mutants) using
404 polyetherimide (PEI). Pseudoviruses supernatants were collected 48hrs after transfection. 3-fold
405 serially diluted plasma (starting at 1:20), HEK293T supernatant (starting at 1:4.5), or mAbs (starting
406 at 10 μg/ml) were mixed with pseudoviruses at 37˚C for 1hr. HEK293T-hACE2 cells (1.5×10^4 per well)
407 were added into the mixture and incubated at 37˚C for 48hrs. Cells were lysed to measure luciferase
408 activity by Bright-Lite Luciferase Assay System (Vazyme Biotech, DD1204-02). The percentages of
409 neutralization were determined by comparing with the virus control. The data were analyzed and
410 plotted with GraphPad Prism.

411 **Competition ELISA**

412 Purified huACE2, CR3022, S309, P2S-2E9, BD55-5483, BD56-1854 and BD55-1205 were labeled
413 with HRP (ProteinTech, PK20001). WT RBD was coated onto 96-well ELISA plates (50 ng/well). After
414 blocking with blocking buffer (PBS with 10% FBS), blocking mAbs were added and incubated at 37
415 ˚C for 1 hr. Then HRP-labeled detecting reagents were added in the presence of blocking mAbs and
416 incubated at 37˚C for 1 hr. The ratio of blocking and detecting reagents was 100:1. After wash, TMB
417 substrate (Sangon Biotech, E661007-0100) was added and incubated at room temperature for 30
418 minutes. Then the reaction was stopped with stop solution and absorbance at 450 nm (OD450) was
419 measured. The percentages of signal reduction caused by blocking mAbs were calculated.

420 **Binding activity measured by FACS**

421 The plasmids encoding spikes of WT, BA.4/5, KP.3 and KP.3 mutants were transfected into HEK293T
422 cells. After 48hr, cells were harvested. To compare the binding activity of germline and mature
423 antibodies to WT and BA.4/5 spikes, cells were incubated with 3-fold serially diluted germline or
424 mature mAbs (starting at 10 μg/ml) for 30 min at 4˚C. To compare the binding with KP.3 and KP.3
425 mutants, cells were incubated with 1 μg/ml mAbs or 10 nM biotinylated ACE2 for 30 min at 4˚C. After
426 wash, cells stained with mAbs were further stained with DAPI and goat anti-human IgG FITC
427 (Proteintech, SA00003-12), whereas cells stained with ACE2 were further stained with DAPI and
428 streptavidin APC (Biolegend, 405243). After wash, cells were analyzed by CytoFLEX (BECKMAN
429 COULTER). FACS data were analyzed with Flowjo V10 to determine the percentages of positive cells.
430 To compare the binding activity of germline and mature antibodies to WT and BA.4/5 spikes, the
431 percentages were ploted with GraphPad Prism. To compare the binding with KP.3 and KP.3 mutants,
432 the percentages for KP.3 mutants were divided by the percentages for KP.3 and the ratios were
433 recorded.

434 **Sequence analysis**

435 Variable regions of antibody heavy and light chains from single B cells were analyzed with IgBlast
436 (https://www.ncbi.nlm.nih.gov/igblast/). Using Python 3.12, clonotypes were analyzed with the Bio,
437 pandas, and numpy packages. Antibodies with same V and J genes and more than 85% similarity in
438 CDR3 (nucleotide sequence) for both heavy and light chains were defined as clones within the same
439 clonotype. Spike sequences, uploaded from June 1 2024 to October 1 2024, were obtained from
440 NCBI Virus. Sequences with lengths outside the range of 1250–1290 or containing 'X' were removed.
441 Sequence alignment was performed using Muscle5, and statistical analysis was conducted with
442 Python 3.12.

443 **Statistics and reproducibility**

444 All statistical analyses were performed with GraphPad Prism. The numbers of biological repeats for

445 each experiment and tests for statistical significance are described in corresponding figure legends.

446 **References**

447 1. S. Tonegawa, Somatic generation of antibody diversity. *Nature* **302**, 575-581 (1983).
448 2. F. D. Batista, N. E. Harwood, The who, how and where of antigen presentation to B cells. *Nat Rev Immunol*
449 **9**, 15-27 (2009).
450 3. G. D. Victora, M. C. Nussenzweig, Germinal Centers. *Annu Rev Immunol* **40**, 413-442 (2022).
451 4. T. Inoue, I. Moran, R. Shinnakasu, T. G. Phan, T. Kurosaki, Generation of memory B cells and their
452 reactivation. *Immunol Rev* **283**, 138-149 (2018).
453 5. K. Roltgen, S. D. Boyd, Antibody and B Cell Responses to SARS-CoV-2 Infection and Vaccination: The End
454 of the Beginning. *Annu Rev Pathol* **19**, 69-97 (2024).
455 6. D. Lapuente, T. H. Winkler, M. Tenbusch, B-cell and antibody responses to SARS-CoV-2: infection,
456 vaccination, and hybrid immunity. *Cell Mol Immunol* **21**, 144-158 (2024).
457 7. H. Qi, B. Liu, X. Wang, L. Zhang, The humoral response and antibodies against SARS-CoV-2 infection. *Nat*
458 *Immunol* **23**, 1008-1020 (2022).
459 8. Z. Ling, C. Yi, X. Sun, Z. Yang, B. Sun, Broad strategies for neutralizing SARS-CoV-2 and other human
460 coronaviruses with monoclonal antibodies. *Sci China Life Sci* **66**, 658-678 (2023).
461 9. H. Liu, I. A. Wilson, Protective neutralizing epitopes in SARS-CoV-2. *Immunol Rev* **310**, 76-92 (2022).
462 10. K. M. Hastie *et al.*, Defining variant-resistant epitopes targeted by SARS-CoV-2 antibodies: A global
463 consortium study. *Science* **374**, 472-478 (2021).
464 11. M. McCallum *et al.*, N-terminal domain antigenic mapping reveals a site of vulnerability for SARS-CoV-2.
465 *Cell* **184**, 2332-2347 e2316 (2021).
466 12. G. Cerutti *et al.*, Potent SARS-CoV-2 neutralizing antibodies directed against spike N-terminal domain
467 target a single supersite. *Cell Host Microbe* **29**, 819-833 e817 (2021).
468 13. M. Yuan *et al.*, Structural basis of a shared antibody response to SARS-CoV-2. *Science* **369**, 1119-1123
469 (2020).
470 14. D. F. Robbiani *et al.*, Convergent antibody responses to SARS-CoV-2 in convalescent individuals. *Nature*
471 **584**, 437-442 (2020).
472 15. Q. Yan *et al.*, Shared IGHV1-69-encoded neutralizing antibodies contribute to the emergence of L452R
473 substitution in SARS-CoV-2 variants. *Emerg Microbes Infect* **11**, 2749-2761 (2022).
474 16. Y. Wang *et al.*, A large-scale systematic survey reveals recurring molecular features of public antibody
475 responses to SARS-CoV-2. *Immunity* **55**, 1105-1117 e1104 (2022).
476 17. C. Gaebler *et al.*, Evolution of antibody immunity to SARS-CoV-2. *Nature* **591**, 639-644 (2021).
477 18. M. Sakharkar *et al.*, Prolonged evolution of the human B cell response to SARS-CoV-2 infection. *Sci*
478 *Immunol* **6**, (2021).
479 19. A. Sokal *et al.*, Maturation and persistence of the anti-SARS-CoV-2 memory B cell response. *Cell* **184**,
480 1201-1213 e1214 (2021).
481 20. Z. Wang *et al.*, mRNA vaccine-elicited antibodies to SARS-CoV-2 and circulating variants. *Nature* **592**,
482 616-622 (2021).

21. J. S. Turner *et al.*, SARS-CoV-2 mRNA vaccines induce persistent human germinal centre responses. *Nature* **596**, 109-113 (2021).
22. W. Kim *et al.*, Germinal centre-driven maturation of B cell response to mRNA vaccination. *Nature* **604**, 141-145 (2022).
23. R. Viana *et al.*, Rapid epidemic expansion of the SARS-CoV-2 Omicron variant in southern Africa. *Nature* **603**, 679-686 (2022).
24. Z. Wang *et al.*, Memory B cell responses to Omicron subvariants after SARS-CoV-2 mRNA breakthrough infection in humans. *J Exp Med* **219**, (2022).
25. J. Quandt *et al.*, Omicron BA.1 breakthrough infection drives cross-variant neutralization and memory B cell formation against conserved epitopes. *Sci Immunol* **7**, eabq2427 (2022).
26. C. I. Kaku *et al.*, Recall of preexisting cross-reactive B cell memory after Omicron BA.1 breakthrough infection. *Sci Immunol* **7**, eabq3511 (2022).
27. T. Weber *et al.*, Enhanced SARS-CoV-2 humoral immunity following breakthrough infection builds upon the preexisting memory B cell pool. *Sci Immunol* **8**, eadk5845 (2023).
28. A. Sokal *et al.*, SARS-CoV-2 Omicron BA.1 breakthrough infection drives late remodeling of the memory B cell repertoire in vaccinated individuals. *Immunity* **56**, 2137-2151 e2137 (2023).
29. C. I. Kaku *et al.*, Evolution of antibody immunity following Omicron BA.1 breakthrough infection. *Nat Commun* **14**, 2751 (2023).
30. C. Q. Huang, S. Vishwanath, G. W. Carnell, A. C. Y. Chan, J. L. Heeney, Immune imprinting and next-generation coronavirus vaccines. *Nat Microbiol* **8**, 1971-1985 (2023).
31. Q. Wang *et al.*, Deep immunological imprinting due to the ancestral spike in the current bivalent COVID-19 vaccine. *Cell Rep Med* **4**, 101258 (2023).
32. T. S. Johnston *et al.*, Immunological imprinting shapes the specificity of human antibody responses against SARS-CoV-2 variants. *Immunity* **57**, 912-925 e914 (2024).
33. M. A. Tortorici *et al.*, Persistent immune imprinting occurs after vaccination with the COVID-19 XBB.1.5 mRNA booster in humans. *Immunity* **57**, 904-911 e904 (2024).
34. A. Yisimayi *et al.*, Repeated Omicron exposures override ancestral SARS-CoV-2 immune imprinting. *Nature* **625**, 148-156 (2024).
35. C. Y. Liang *et al.*, Imprinting of serum neutralizing antibodies by Wuhan-1 mRNA vaccines. *Nature* **630**, 950-960 (2024).
36. I. Paciello *et al.*, Antigenic sin and multiple breakthrough infections drive converging evolution of COVID-19 neutralizing responses. *Cell Rep* **43**, 114645 (2024).
37. L. Li *et al.*, Breakthrough infection elicits hypermutated IGHV3-53/3-66 public antibodies with broad and potent neutralizing activity against SARS-CoV-2 variants including the emerging EG.5 lineages. *PLoS Pathog* **19**, e1011856 (2023).
38. Q. Wang *et al.*, Antibody neutralisation of emerging SARS- CoV-2 subvariants: EG.5.1 and XBC.1.6. *Lancet Infect Dis* **23**, E397-E398 (2023).
39. M. Yuan *et al.*, A highly conserved cryptic epitope in the receptor binding domains of SARS-CoV-2 and SARS-CoV. *Science* **368**, 630-633 (2020).
40. D. Pinto *et al.*, Cross-neutralization of SARS-CoV-2 by a human monoclonal SARS-CoV antibody. *Nature* **583**, 290-295 (2020).
41. B. Ju *et al.*, Infection with wild-type SARS-CoV-2 elicits broadly neutralizing and protective antibodies against omicron subvariants. *Nat Immunol* **24**, 690-699 (2023).
42. Y. L. Cao *et al.*, Rational identification of potent and broad sarbecovirus-neutralizing antibody cocktails

527 from SARS convalescents. *Cell Reports* **41**, (2022).
528 43. Y. L. Cao *et al.*, Imprinted SARS-CoV-2 humoral immunity induces convergent Omicron RBD evolution.
529 *Nature* **614**, 521-+ (2023).
530 44. R. Kotaki *et al.*, Repeated Omicron exposures redirect SARS-CoV-2-specific memory B cell evolution
531 toward the latest variants. *Sci Transl Med* **16**, eadp9927 (2024).
532 45. W. B. Alsoussi *et al.*, SARS-CoV-2 Omicron boosting induces de novo B cell response in humans. *Nature*
533 **617**, 592-+ (2023).
534 46. X. Rao *et al.*, Defining a de novo non- RBM antibody as RBD-8 and its synergistic rescue of immune-
535 evaded antibodies to neutralize Omicron SARS- CoV-2. *P Natl Acad Sci USA* **120**, (2023).
536 47. F. Jian *et al.*, Evolving antibody response to SARS-CoV-2 antigenic shift from XBB to JN.1. (2024) bioRxiv,
537 https://doi.org/10.1101/2024.04.19.590276.
538 48. M. Korenkov *et al.*, Somatic hypermutation introduces bystander mutations that prepare SARS-CoV-2
539 antibodies for emerging variants. *Immunity* **56**, (2023).
540 49. M. Bruhn *et al.*, Diversification of the VH3-53 immunoglobulin gene segment by somatic hypermutation
541 results in neutralization of SARS-CoV-2 virus variants. *Eur J Immunol* **54**, (2024).
542 50. Z. Wang *et al.*, Ancestral SARS-CoV-2 immune imprinting persists on RBD but not NTD after sequential
543 Omicron infections. (2024) bioRxiv, https://doi.org/10.1101/2024.05.30.596664.

544 **Acknowledgements**

545 The authors thank the donors for providing peripheral blood. This work is supported by the National
546 Key Plan for Scientific Research and Development of China (Grant No. 2022YFC2305800) and the
547 National Natural Science Foundation of China (Grant No. 32200765, Grant No. 32370941).

548 **Author contributions**

549 Conceptualization, L.J. and T.Z.; Validation, X.C., L.L., R.D., Z.W.; Formal Analysis, X.C., L.L., R.D.,
550 Z.W. and Y.L.; Investigation, X.C., L.L., R.D., Z.W., Y.L., Y.S., R.Q., H.F., L.H., X.C., M.L., X.H. and
551 L.J.; Writing – Original Draft, X.C., L.L., R.D., Z.W., Y.L., L.J. and T.Z.; Writing – Review & Editing, L.J.
552 and T.Z.; Visualization, X.C., L.L., Z.W. and Y.L.; Supervision, L.J. and T.Z.; Funding Acquisition, L.J.
553 and T.Z..

554 **Competing interests**

555 L.J., T.Z., X.C., L.L., R.D. and Z.W. are inventors on a patent application for antibodies including
556 KXD350, KXD352, KXD355, KXD358. The other authors have no competing interests.
557

558 **Figures and figure legends**

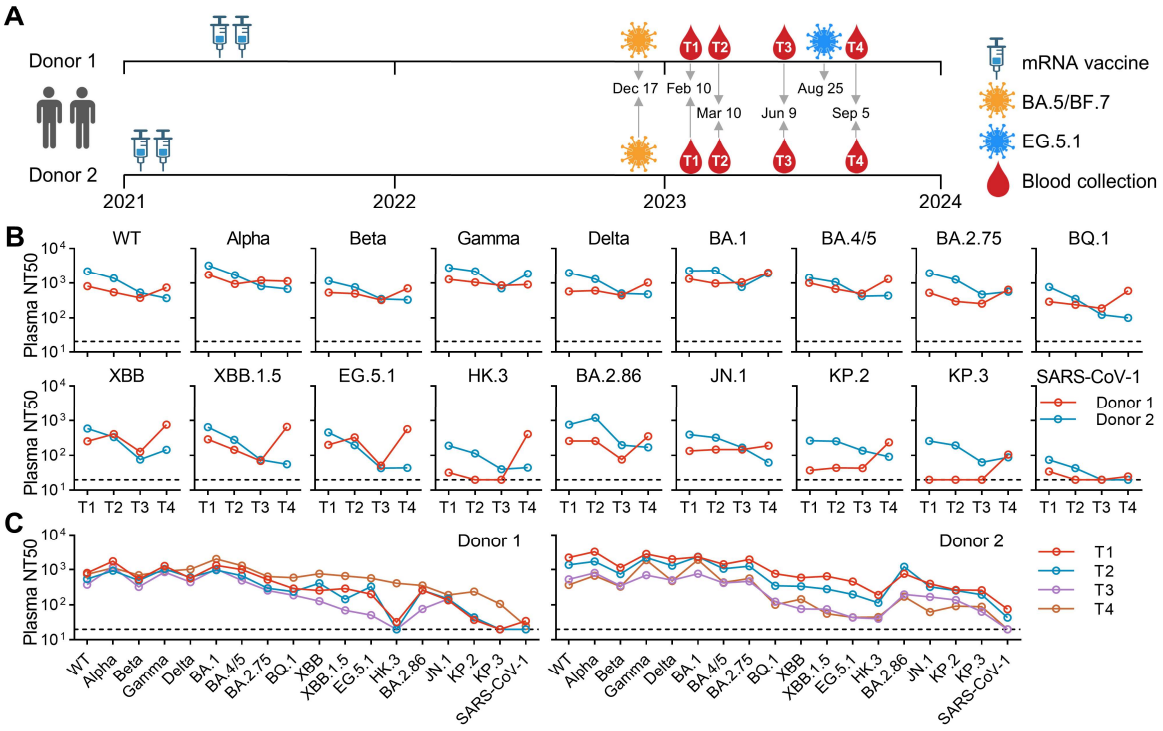

559

560 **Figure 1. Longitudinal analysis of plasma neutralizing antibody responses in two individuals.**

561 (A) Basic information of donors and samples. (B, C) Summary of plasma neutralizing antibody titers

562 (NT50). NT50s are calculated with results from three independent experiments, in which duplicates

563 are performed.

564

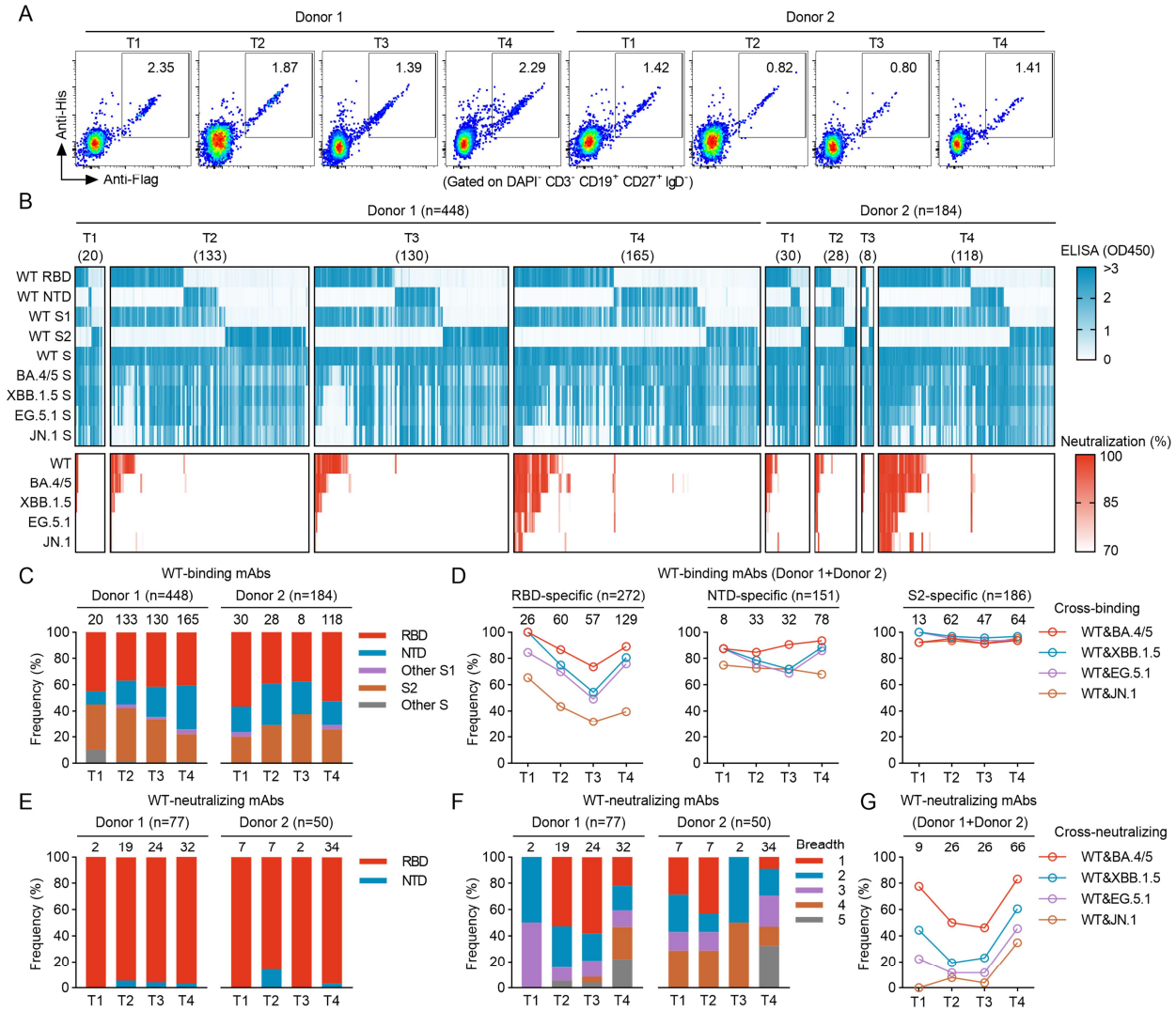

Figure 2. Isolation and characterization of mAbs.

(A) FACS plots representing the percentages of WT-spike-specific B cells in DAPI$^-$CD3$^-$CD19$^+$CD27$^+$IgD$^-$ B cells. (B) ELISA and neutralization results of 632 mAbs from two donors. Supernatant of HEK293T is tested against 9 antigens by ELISA, and tested against 5 pseudoviruses by neutralization assay. For ELISA, supernatant is not diluted. For neutralization, supernatant is diluted by 4.5 folds. The results are mean values from two independent experiments, in which duplicates are performed. (C) Frequencies of mAbs targeting each domain among mAbs binding to WT spike (WT-binding mAbs). (D) Frequencies of cross-binding mAbs among RBD-specific, NTD-specific, and S2-specific mAbs. (E) Frequencies of mAbs targeting RBD or NTD among mAbs

575 neutralizing WT pseudoviruses (WT-neutralizing mAbs). (F) Frequencies of mAbs with different

576 neutralizing breadth. Breadth indicates the number of pseudoviruses can be neutralized by mAbs. (G)

577 Frequencies of cross-neutralizing mAbs.

578

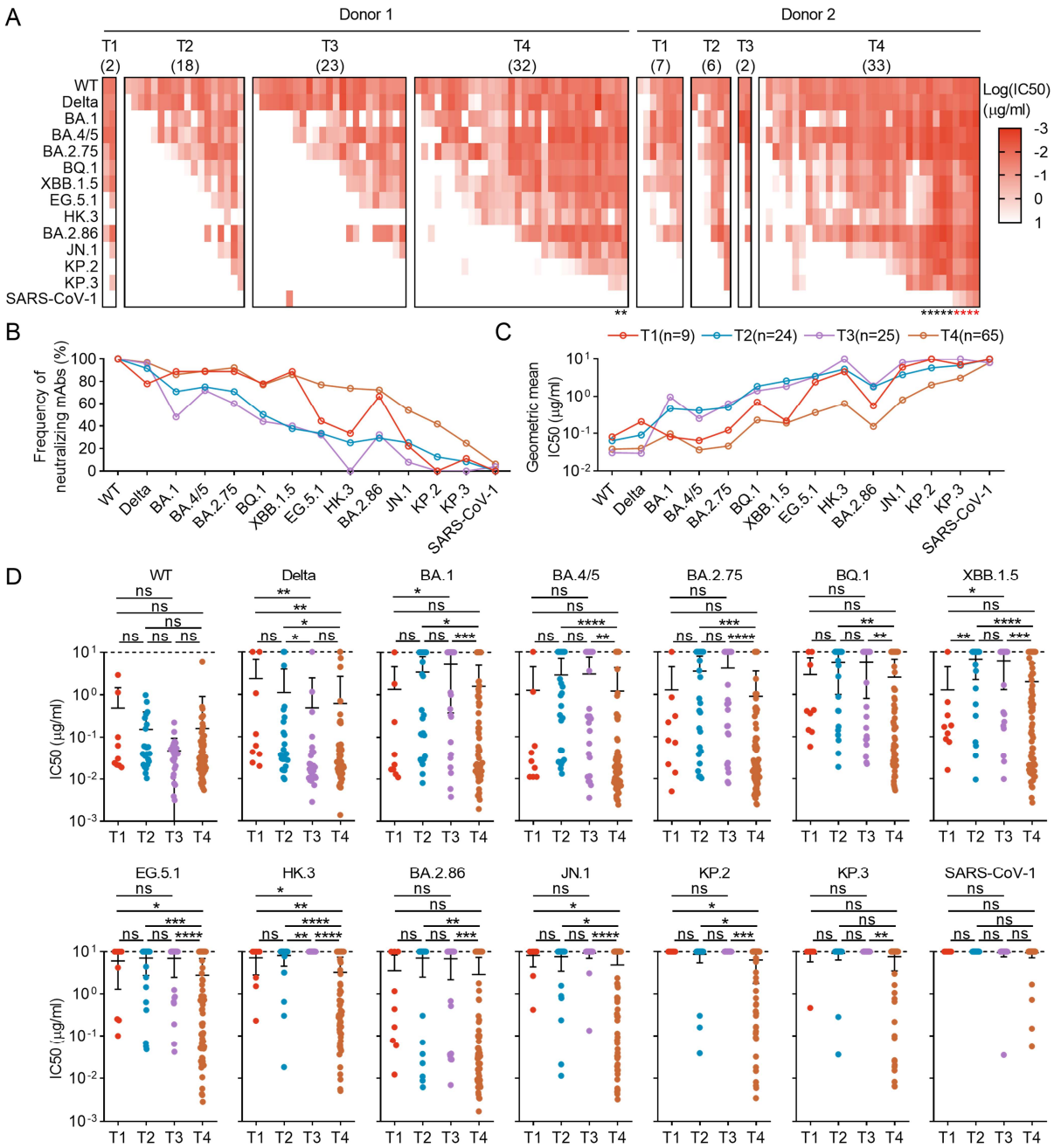

Figure 3. Neutralizing potency of mAbs against SARS-CoV-2 and SARS-CoV-1. (A) IC50s of mAbs against 14 pseudoviruses. The highest antibody concentration used to determine IC50 is 10 μg/ml. IC50s are calculated with results from two independent experiments, in which duplicates are performed. The black asterisk indicates mAbs with broadly neutralizing activity against SARS-CoV-2 variants from WT to KP.3. The red asterisk indicates mAbs with broadly neutralizing activity against SARS-CoV-2 and SARS-CoV-1. (B) Frequencies of neutralizing mAbs against each pseudoviruses

586 among mAbs from T1 to T4. (C) Geometric mean IC50s of mAbs from T1 to T4 against each

587 pseudoviruses. (D) Comparison of IC50s. Statistical analysis is performed by Mann-Whitney test. ns

588 (not significant) $P > 0.05$, *$P < 0.05$, **$P < 0.01$, ***$P < 0.001$, ****$P < 0.0001$.

589

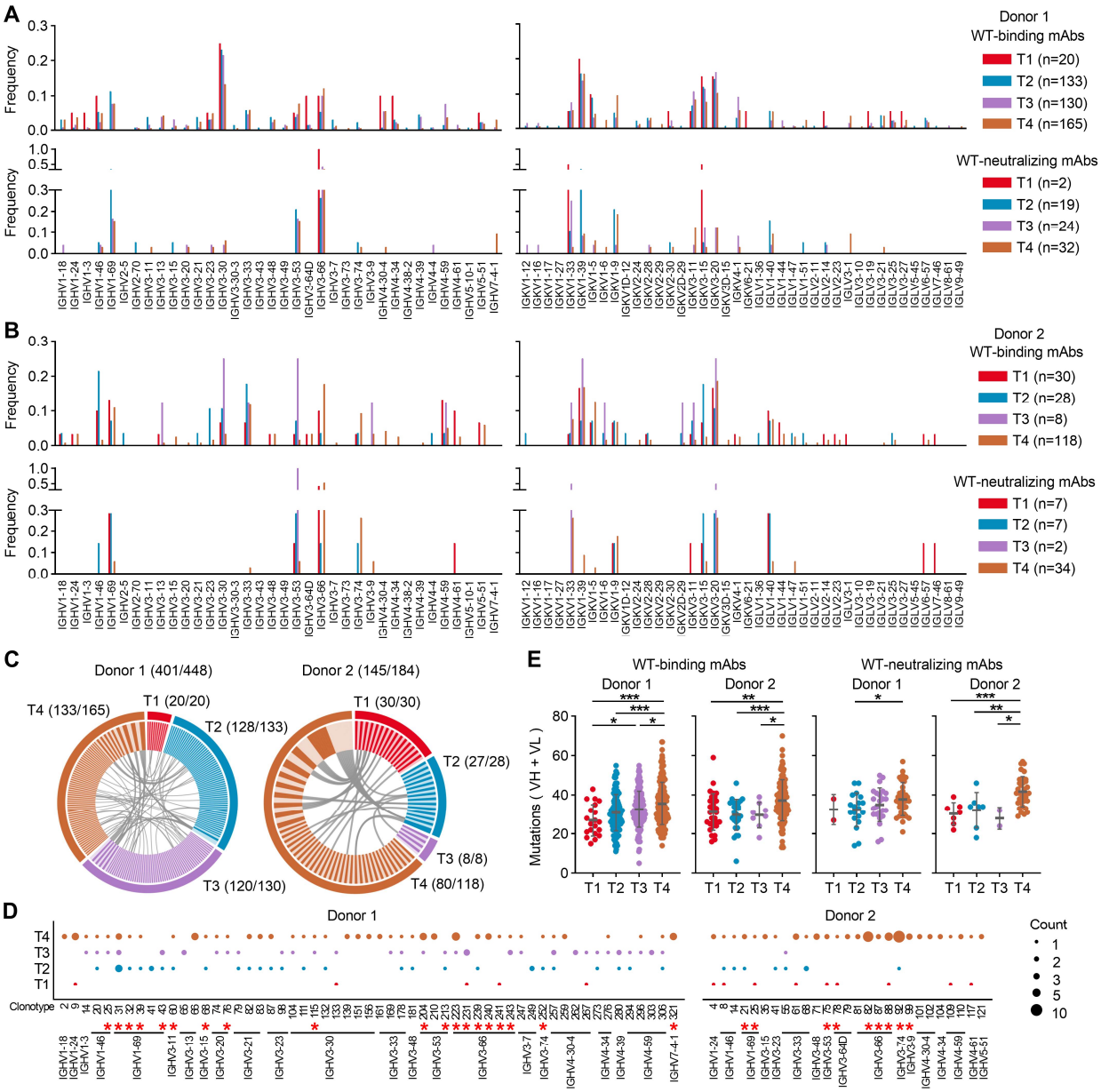

Figure 4. Sequence analysis. (A, B) Frequencies of V genes used by mAbs binding to WT spike (WT-binding mAbs) and mAbs neutralizing WT pseudoviruses (WT-neutralizing mAbs) from Donor 1 and Donor 2. (C) Clonotype analysis of WT-binding mAbs from Donor 1 and Donor 2. Values in parentheses indicate number of clonotypes/number of mAbs. Different clonotypes are distinguished by alternating colors, and identical clonotypes across different time points are connected by gray lines. (D) Bubble plot of clonotypes comprising two or more mAbs. Dot size indicates number of mAbs. The red asterisk indicates clonotypes containing neutralizing mAbs. (E) Somatic hypermutation on

598 variable regions of heavy and light chains based on DNA sequences. Statistical analysis is performed

599 by two-tailed unpaired T test. *P<0.05, **P < 0.01, ***P < 0.001.

600

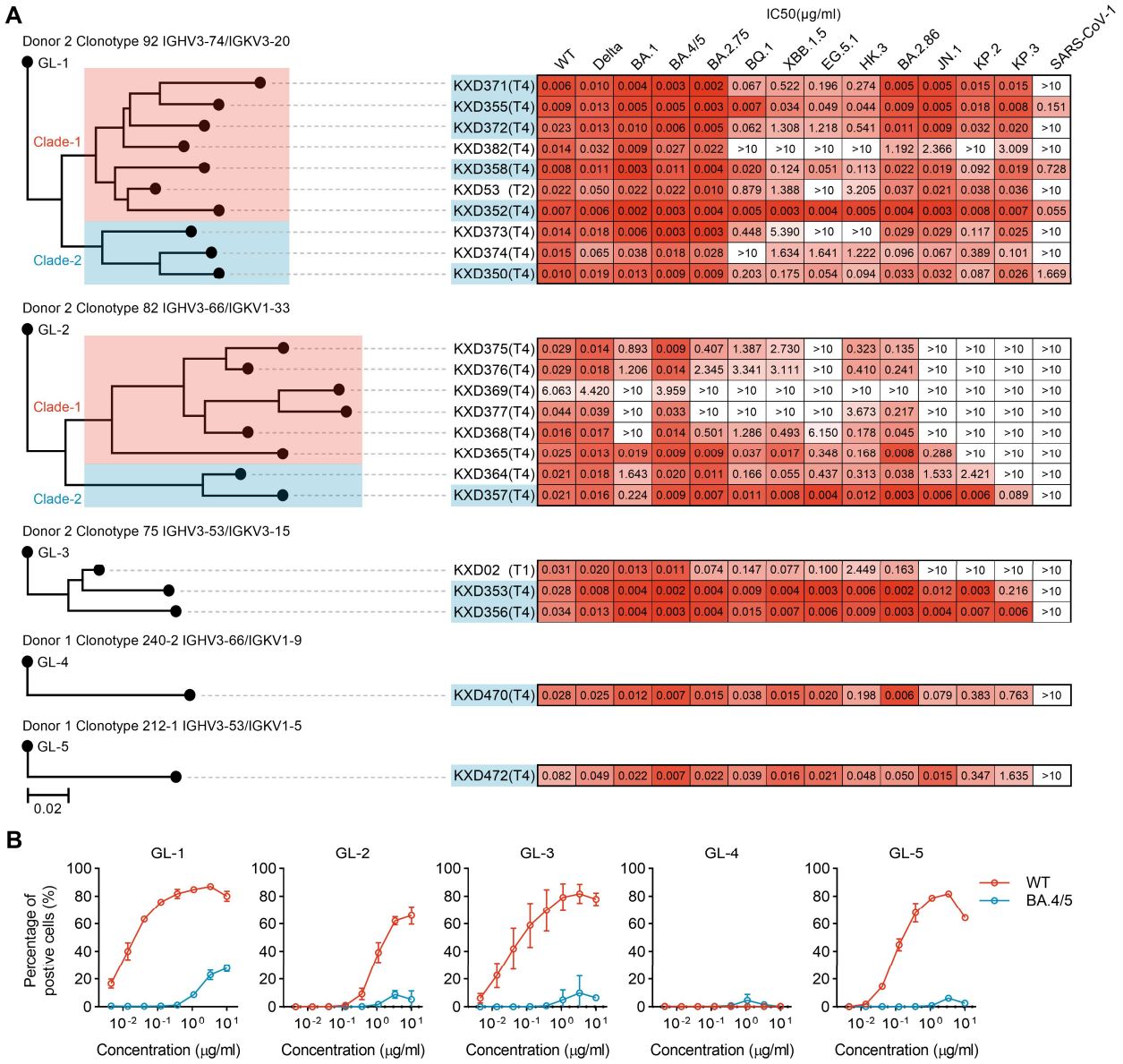

Figure 5. Clonotypes containing mAbs with extraordinary neutralizing breadth and potency. (A) Maximum-likelihood phylogenetic trees of each clonotype and IC50s of each mAbs. (B) Binding of germline antibodies to WT and BA.4/5 spikes expressed on HEK293T cells.

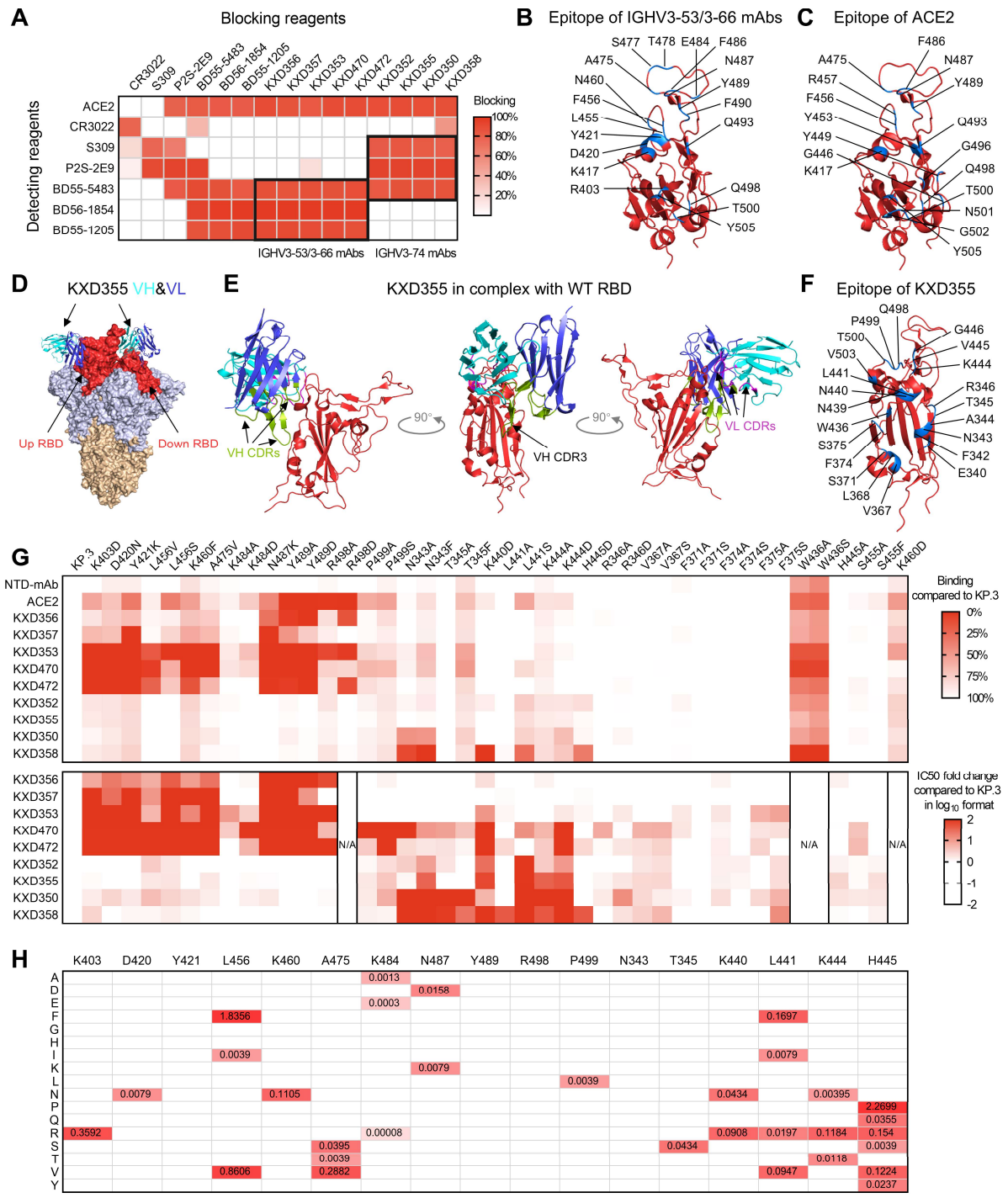

606

607 **Figure 6. Epitope mapping and escape mutations of mAbs with extraordinary neutralizing**

608 **breadth and potency.** (A) Competition ELISA. The blocking indicates signal (OD450) reduced by

609 blocking mAbs. The results are mean values from two independent experiments, in which duplicates

610 are performed. (B) Epitope of IGHV3-53/3-66 mAbs on WT RBD (PDB: 7A94). (C) Epitope of ACE2

611 on WT RBD (PDB: 7A94). (D) The predicted structure of KXD355 in complex with WT RBD is aligned
612 to up RBD and down RBD on WT spike (PDB: 7A94). (E) Detailed view of KXD355 in complex with
613 WT RBD. (F) Epitope of KXD355 on WT RBD (PDB: 7A94). (G) Binding and neutralizing activities
614 against single-mutated KP.3. The binding activities are measured by FACS. NTD-mAb, a mAb
615 targeting NTD, is used to evaluate the expression levels of KP.3 mutants. The results of binding
616 activities are mean values from two independent experiments. For neutralizing activities, IC50s are
617 calculated with results from two independent experiments, in which duplicates are performed. N/A
618 (not applicable) indicates that neutralization assay is not done because we are not able to generate
619 pseudoviruses for the mutant. (H) Frequencies of mutations on the indicated sites among a total of
620 25332 spike sequences with KP.3 as reference. The confirmed escape mutations of IGHV3-53/3-66
621 and IGHV3-74 bnAbs are located on these sites.
622

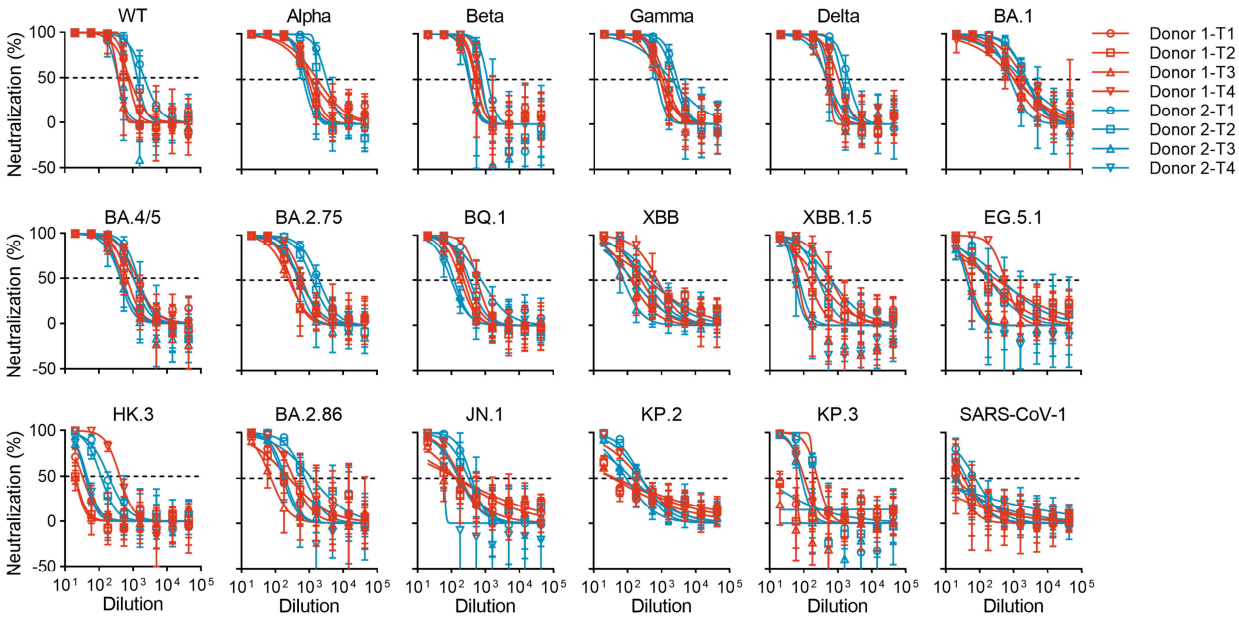

Figure S1. Plasma neutralizing antibody titers. (A) Plasma neutralizing antibody titers against a panel of pseudoviruses. The data are represented as mean ± SD and they are from three independent experiments, in which duplicates are performed. The published data for plasma from T1 are not used here. Instead, we measured the neutralizing tiers of plasma from T1 again, along with plasma from other time points.

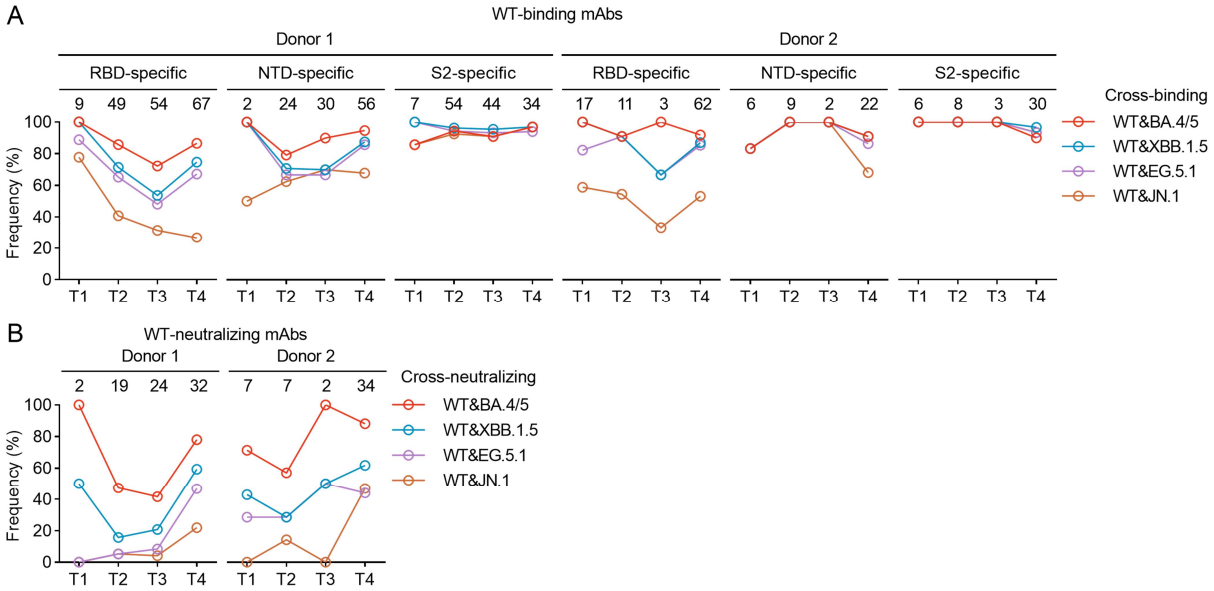

Figure S2. Cross-binding and cross-neutralizing mAbs from Donor 1 and Donor 2. (A) Frequencies of cross-binding mAbs among RBD-specific, NTD-specific, and S2-specific mAbs from Donor 1 and Donor 2. (B) Frequencies of cross-neutralizing mAbs from Donor 1 and Donor 2.

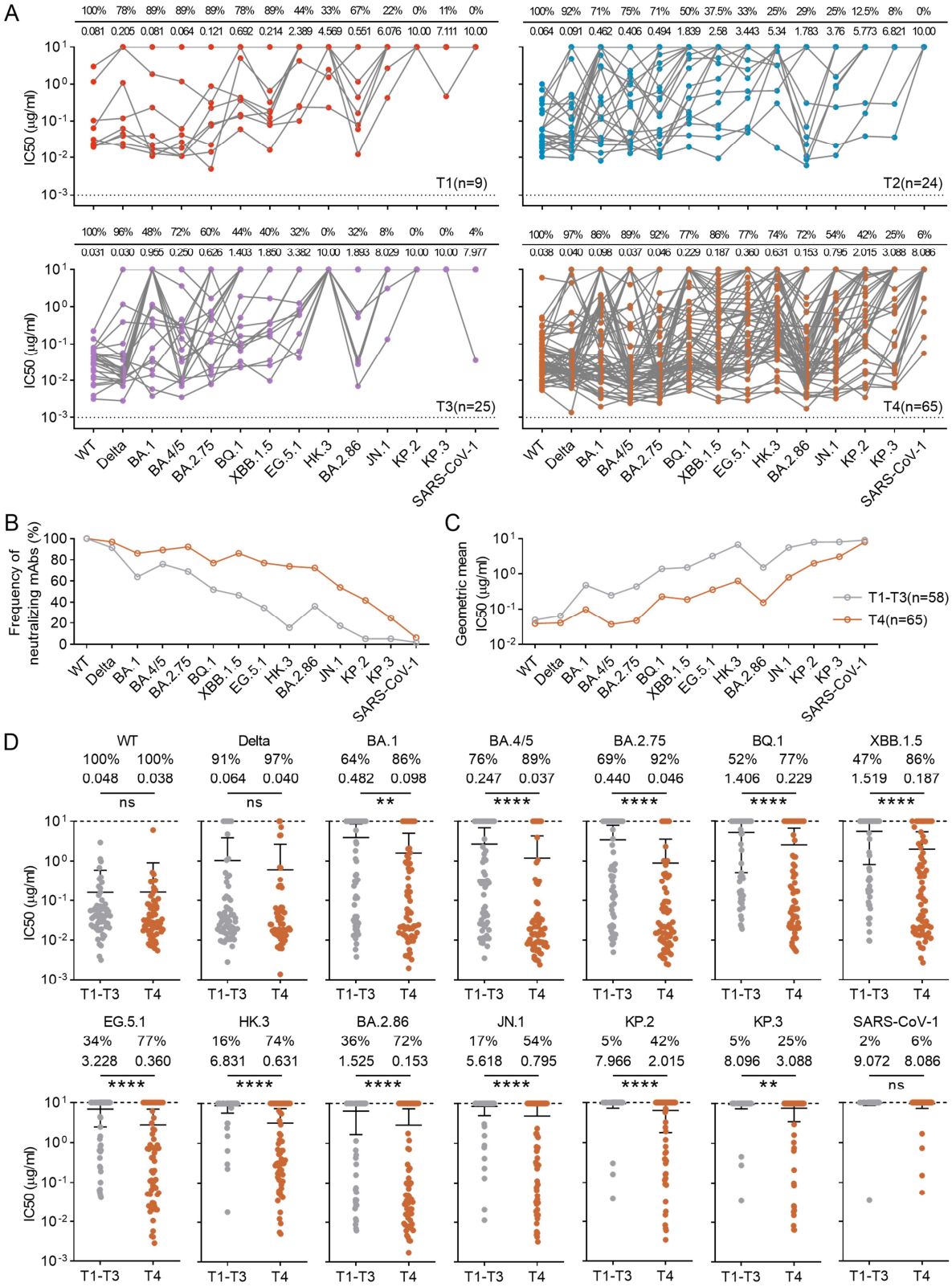

Figure S3. IC50s of mAbs. (A) Summary of IC50s. The numbers below the line indicate the geometric mean IC50s and the numbers above the line represent the percentage of mAbs that is able to

638 neutralize the corresponding pseudoviruses (IC50 below 10 μg/ml). (B) Frequencies of neutralizing
639 mAbs against each pseudoviruses among T1-T3 group and T4 group. (C) Geometric mean IC50s of
640 mAbs among T1-T3 group and T4 group. (D) Comparison of IC50s. The numbers below and above
641 indicate the geometric mean IC50s and the percentages of neutralizing mAbs, respectively. Statistical
642 analysis is performed by Mann-Whitney test. ns (not significant) $P > 0.05$, **$P < 0.01$, ****$P < 0.0001$.
643

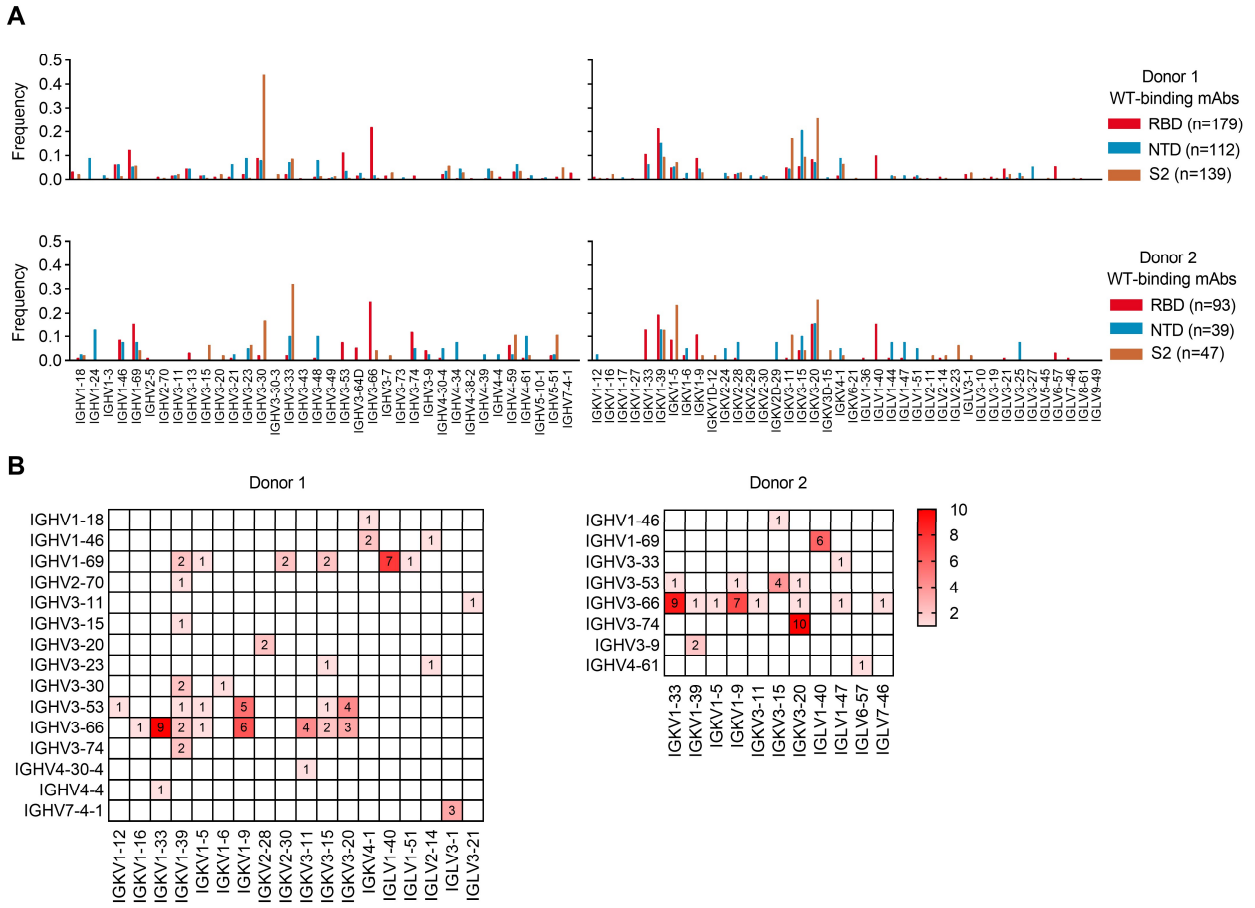

Figure S4. Analysis of V gene usage. (A) Frequencies of V genes used by mAbs targeting RBD, NTD and S2. (B) Paring of V genes for heavy and light chains in neutralizing mAbs. The number in each box indicates the count of mAbs using the corresponding pair.

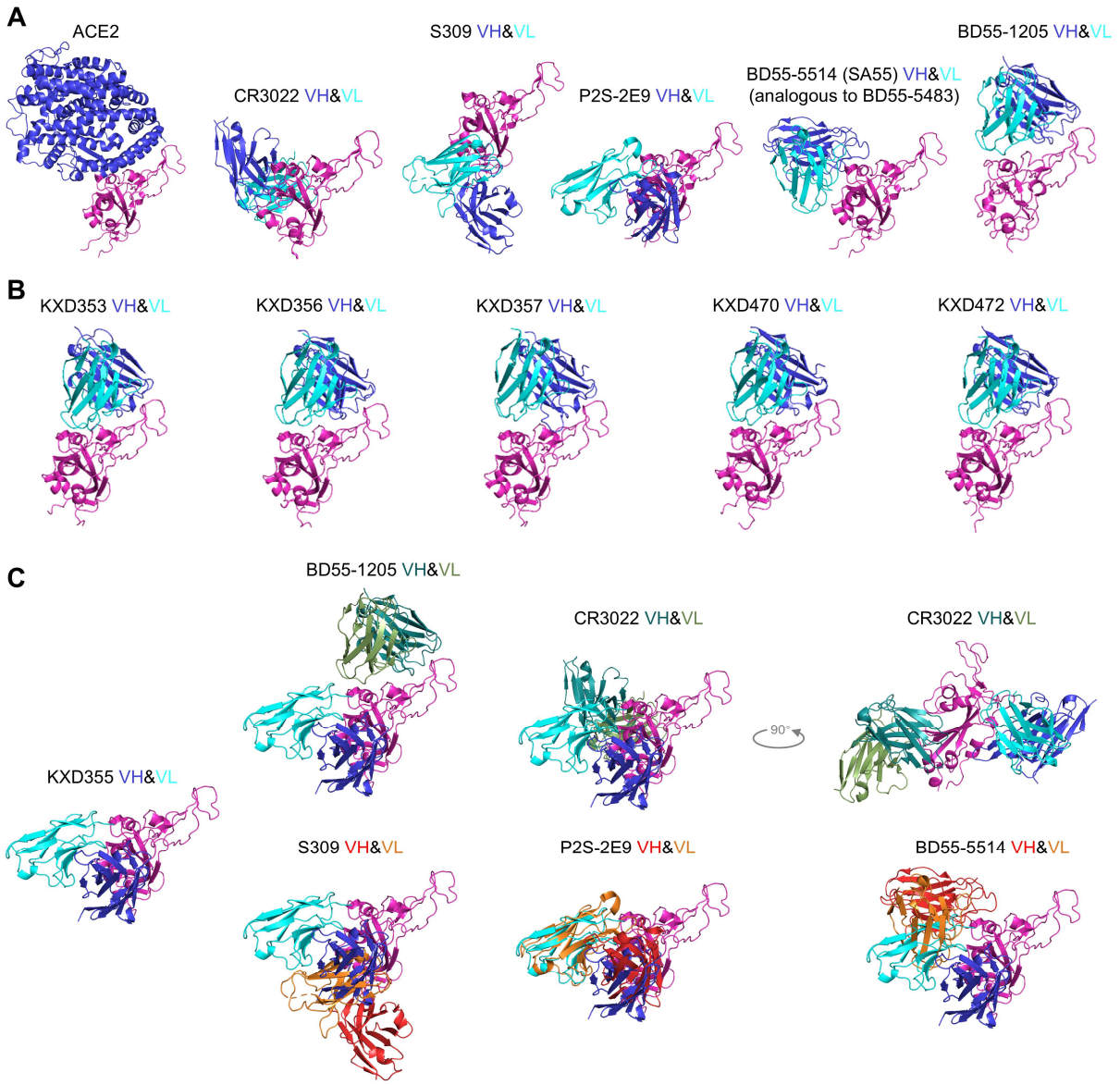

Figure S5. Published structures and predicted structures. (A) The published structures of ACE2 (PDB: 7A94), CR3022 (PDB: 6W41), S309 (PDB: 7TLY), P2S-2E9 (PDB: 7XSA), BD55-5514 (PBD: 7Y0W), BD55-1205 (PDB: 8XEA) in complex with RBD. (B) The predicted structures of KXD353, KXD356, KXD357, KXD470 and KXD472 in complex with WT RBD. (C) The predicted structure of KXD355 in complex with WT RBD is aligned with published structures of CR3022, S309, P2S-2E9, BD55-5514 and BD55-1205.

	KXD356	KXD357	KXD353	KXD470	KXD472	KXD352	KXD355	KXD350	KXD358
KP.3	0.006	0.089	0.216	0.763	1.635	0.007	0.008	0.026	0.019
K403D	0.043	>10	>10	>10	>10	0.006	0.009	0.041	0.05
D420N	0.126	2.407	>10	>10	>10	0.005	0.007	0.067	0.016
Y421K	0.08	>10	>10	>10	>10	0.002	0.005	0.043	0.023
L456V	0.038	0.958	1.114	>10	>10	0.022	0.014	0.117	0.023
L456S	0.243	>10	>10	>10	>10	0.012	0.015	0.072	0.028
K460F	0.057	>10	3.384	>10	>10	0.004	0.008	0.053	0.023
A475V	0.148	>10	>10	>10	>10	0.005	0.013	0.039	0.016
K484A	0.003	0.015	2.174	2.529	1.612	0.003	0.005	0.018	0.006
K484D	0.007	0.03	0.631	>10	9.051	0.005	0.009	0.037	0.012
N487K	>10	>10	>10	>10	>10	0.006	0.008	0.044	0.017
Y489A	>10	>10	>10	>10	>10	0.003	0.002	0.006	0.004
Y489D	>10	0.986	>10	>10	>10	0.001	0.002	0.008	0.002
R498A	0.385	0.017	>10	3.665	>10	0.004	0.006	0.029	0.011
R498D					N/A				
P499A	0.004	0.053	0.086	>10	5.506	0.008	0.013	0.042	0.026
P499S	0.008	0.077	0.195	>10	>10	0.016	0.029	0.162	0.024
N343A	0.003	0.029	0.022	>10	3.81	0.021	0.01	>10	>10
N343F	0.004	0.051	0.061	7.918	2.951	0.063	0.273	>10	>10
T345A	0.004	0.035	0.104	6.648	3.247	0.013	0.005	>10	1.66
T345F	0.003	0.049	0.05	3.132	2.047	0.001	0.001	>10	0.484
K440D	0.013	0.074	2.37	>10	>10	0.191	0.55	0.141	>10
L441A	0.003	0.095	0.263	0.361	3.986	0.004	0.004	0.013	0.852
L441S	0.004	0.066	0.162	9.55	1.348	>10	>10	>10	>10
K444A	0.008	0.048	0.181	4.152	5.256	0.023	0.297	5.636	0.907
K444D	0.003	0.011	0.366	>10	>10	0.072	0.382	>10	>10
H445D	0.003	0.095	0.263	0.361	3.986	0.004	0.004	0.013	0.852
R346A	0.001	0.023	0.164	5.175	1.807	0.002	0.01	0.042	0.019
R346D	0.002	0.009	0.358	0.803	2.898	0.006	0.014	0.35	0.037
V367A	0.005	0.026	0.039	4.553	3.388	0.013	0.02	0.064	0.056
V367S	0.004	0.045	0.071	4.755	4.669	0.014	0.02	0.04	0.103
F371A	0.003	0.017	0.373	1.352	0.94	0.004	0.007	0.033	0.009
F371S	0.003	0.007	0.08	0.303	0.241	0.005	0.005	0.021	0.005
F374A	0.008	0.016	0.385	0.985	2.43	0.01	0.011	0.054	0.018
F374S	0.004	0.006	0.1	0.39	0.293	0.01	0.01	0.019	0.016
F375A	0.004	0.073	1.254	1.477	4.554	0.006	0.007	0.063	0.018
F375S	0.002	0.077	1.785	1.608	1.025	0.015	0.017	0.151	0.266
W436A									
W436S					N/A				
H445A	0.008	0.027	0.134	0.773	0.265	0.009	0.021	0.049	0.02
S455A	0.004	0.062	0.101	2.99	7.856	0.008	0.009	0.045	0.013
S455F	0.005	0.012	0.12	0.621	0.102	0.009	0.016	0.047	0.026
K460D					N/A				

Figure S6. IC50s (μg/ml)against KP.3 mutants.

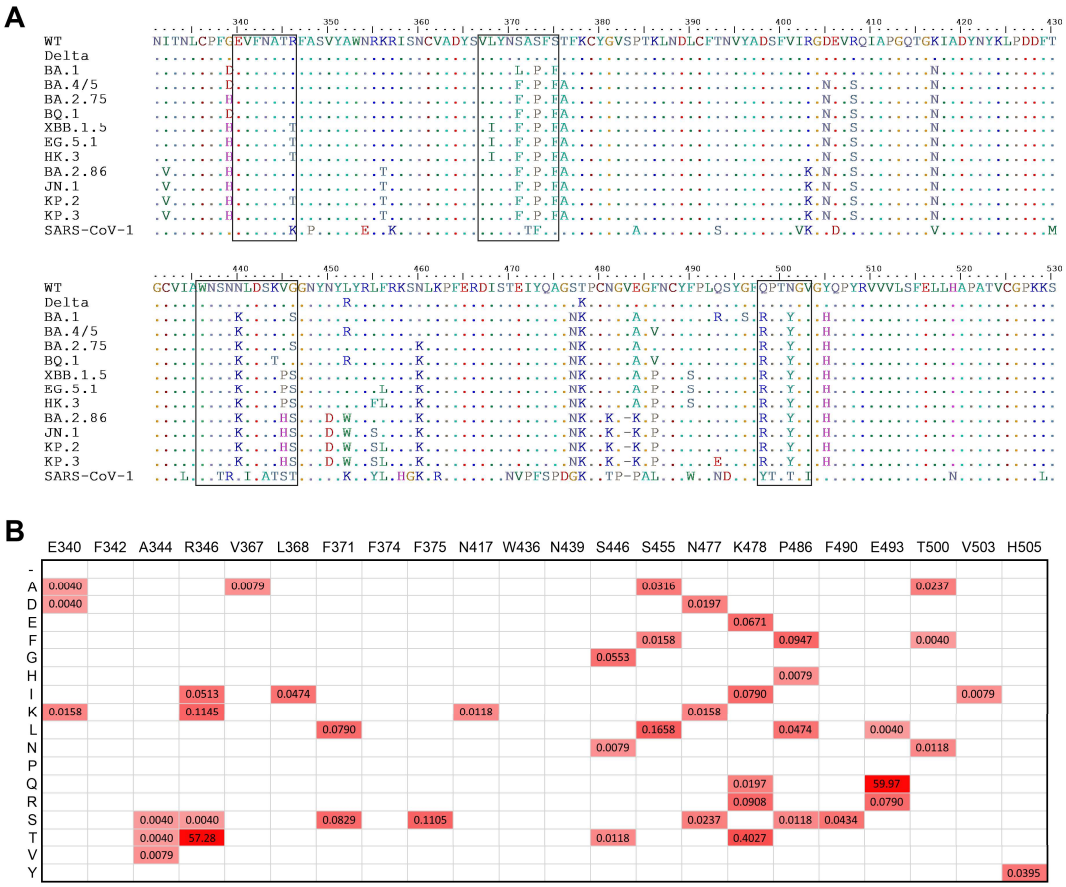

Figure S7. Variations on the epitopes of IGHV3-53/3-66 and IGHV3-74 mAbs. (A) Alignment of RBD sequences from SARS-CoV-2 variants and SARS-CoV-1 tested in neutralization assay. The epitopic regions of IGHV3-74 mAbs are indicated by black frames. (B) Frequencies of mutations on the indicated sites among a total of 25332 spike sequences with KP.3 as reference. These sites are within the epitopes of IGHV3-53/3-66 and IGHV3-74 mAbs while escape mutations have not been identified on these sites.